Available online at www.sciencedirect.com

ScienceDirect

journal homepage: www.elsevier.com/locate/he

Investigation of the correlation effects of catalyst loading and ionomer content in an anode electrode on the performance of polymer electrode membrane water electrolysis

Yeonghwan Jang [a,1], *Changwook Seol* [b,1], *Sang Moon Kim* [b,*], *Segeun Jang* [a,**]

[a] *School of Mechanical Engineering, Kookmin University, Seoul, 02707, Republic of Korea*
[b] *Department of Mechanical Engineering, Incheon National University, Incheon, 22012, Republic of Korea*

HIGHLIGHTS

- MEAs with the cross combination of catalyst loading and ionomer content is prepared.
- A correlation effect of the two factors in the PEMWE system is thoroughly investigated.
- Coupled effect induces electrode porosity change and highly affects the mass transfer.
- 6.882 A cm^{-2} at 2.05 V with 0.5 mg_{IrO_2} and ionomer content of 10 wt% is achieved.

GRAPHICAL ABSTRACT

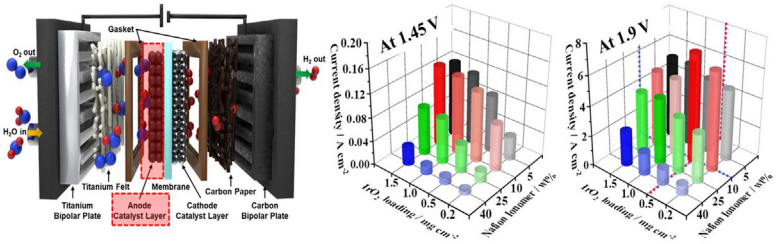

ARTICLE INFO

Article history:
Received 9 November 2021
Received in revised form
26 January 2022
Accepted 3 April 2022
Available online 7 May 2022

Keywords:
Polymer electrolyte membrane water electrolysis
Ionomer content
Catalyst loading

ABSTRACT

In this study, the correlation effect of catalyst loading (L_c) and ionomer content (C_{iono}) on the performance of polymer electrolyte membrane water electrolysis (PEMWE) is investigated. Sixteen membrane electrode assemblies are constructed and electrochemically evaluated using a cross-combination of two factors. Although the coupling of the two factors does not significantly affect the performance at a low working voltage, the effect is dominant at a high working voltage. Based on the establishment of correlations between the changes in the contributing factors (including the ionomer fraction, thickness, and porosity) caused by variations in the two factors, the effects on the kinetic, ohmic, and mass transfer overpotential are estimated and analyzed. Since the C_{iono} and L_c simultaneously affect the porosity, the required C_{iono} for achieving the best performance changes according to the L_c and vice versa. Additionally, a rapid drop in performance when the C_{iono} exceeds 25 wt% is due to the inhibited electron transfer in electrode and interface between the electrode and

* *Corresponding author.*
** *Corresponding author.*
E-mail addresses: ksm7852@inu.ac.kr (S.M. Kim), sjang@kookmin.ac.kr (S. Jang).
[1] These authors contributed equally to this work.
https://doi.org/10.1016/j.ijhydene.2022.04.019

Correlation effects
High-performance

porous transport layers, and a critical ionomer concentration is proposed. Finally, high-performance PEMWE (6.882 A cm^{-2} at 2.05 V) is achieved with a low L_c of 0.5 mg cm^{-2} and a C_{iono} of 10 wt%.

Introduction

With strict carbon emission regulations in place to resolve the issue of accelerating climate change, research on environmentally sound energy sources that can replace fossil fuels has been actively conducted worldwide [1,2]. Due to its advantages, i.e., dynamic capability and broad operational current-density range, polymer electrolyte membrane water electrolysis (PEMWE) can be suitably coupled with fluctuating renewable energy sources, e.g., solar and wind, and convert the extra electricity into hydrogen (H_2) for long-term storage [3]. In addition, H_2 gas generated through PEMWE can be employed as a reactant for generating electricity using fuel cells incorporated into diverse systems including vehicles and power plants [4]. However, more than 95% of H_2 production is currently derived from non-environmentally friendly methods including steam methane reformation, crude oil cracking, and coal gasification, with carbon dioxide (CO_2), carbon monoxide (CO), and methane (CH_4) being generated during these processes [5,6]. Although PEMWE has high efficiency and is environmentally friendly (as it uses only water and electricity), it still accounts for less than 4% of overall H_2 production due to its high capital and operational costs, which are associated with its overall system and electricity consumption [7–9].

To render PEMWE economically viable, the material costs should be reduced, and the performance of the system should be increased [4,10–12]. The US Department of Energy (DOE) suggests that the overall challenge for H_2 production is cost and aims to develop technologies that can produce $2/kg by 2025 and $1/kg by 2030 [13]. To achieve this goal, optimizing the membrane electrode assembly (MEA) of PEMWE with the minimal use of expensive catalysts and ionomers while securing high performance is necessary. Due to the rapid H_2 evolution reaction (HER) kinetics at the cathode, it may be possible to achieve a reduction of platinum loading amounts to several μg cm^{-2} without a significant decrease in performance [10]. Concurrently, the sluggish kinetics of the oxygen (O_2) evolution reaction (OER) kinetics at the anode are orders of magnitude slower. Therefore, high loadings of the anode catalyst iridium (IV) oxide (IrO_2; 1–4 mg cm^{-2}) are generally used [7,12]. As an efficient catalyst for OER under acidic operating conditions, IrO_2 is 10 times more scarce than platinum and only attainable as a byproduct of copper, nickel, and platinum (Pt) mining [4,10]. To reduce the capital expense of PEMWE systems, the reduction of IrO_2 loading is highly necessary to secure a sufficiently high performance for the reduction of electricity consumption. To reduce the IrO_2 loading amount, a significant number of studies have employed supporting materials that maximize IrO_2 dispersion, such as titanium (Ti) dioxide [14], tin (IV) oxide [15], and Ta_xO_2 [16]. However, most of these supports have demonstrated instability in oxidizing environments [12,17]. As another approach, systemic studies investigated the effects of different IrO_2 loadings (with a fixed ionomer content [C_{iono}]) on PEMWE performance [4,12]; these studies were able to reduce the IrO_2 loading to below 1 mg cm^{-2}. In addition, since the structure of the catalyst layer (CL) in the MEA comprises IrO_2 and a proton-conducting ionomer (i.e., typically a Nafion ionomer), the influence of the C_{iono} in the anode CL on PEMWE performance has been investigated using different levels of C_{iono} to achieve high performance (voltage efficiency) when using the same IrO_2 loading [18]. An optimal ionomer use of 11.6 wt% with an IrO_2 loading of 2.0 mg cm^{-2} was determined by analyzing the structure of the CL and PEMWE overpotentials.

It is important to optimize the CL considering the coupling effects of IrO_2 loading and the C_{iono} to reduce the IrO_2 use and attain high performance; some studies have, however, investigated the correlation effects between catalyst loading (L_c) and C_{iono} in the anode on the performance of PEMWE. In this study, to achieve high PEMWE performance with the minimal use of IrO_2, a comprehensive experimental study using 16 MEAs with different L_c and C_{iono} values was conducted by cross combination. For systemic analysis of kinetic, ohmic, and mass transfer overpotentials, we related these with contributing factors, such as the number of active sites, ionomer volume fraction, and thickness and porosity of the CL, based on the variation of the L_c and C_{iono}. The contributing factors were characterized using high-frequency resistance (HFR) analysis, scanning electron microscopy (SEM) observations, electrochemical impedance spectroscopy (EIS) measurements, and cyclic voltammetry (CV) measurements, with variations in L_c and C_{iono}. Based on an analysis of the relationship between the contributing factors and each overpotential, the optimized L_c and C_{iono} for high performance at low and high voltages were determined. Additionally, the inhibited electron transfer effect when a large amount of ionomers were used was observed and verified through the electrochemical analysis.

Experimental section

Preparation of the membrane electrode assembly and the assembly of a single cell

Membrane electrode assemblies with an active area of 5 cm^2 were prepared using a spraying method and different catalyst ink solutions. First, the cathode electrode was prepared using the same spraying method with platinum on carbon (Pt/C)

catalyst ink comprising Pt/C (40 wt%; Johnson Matthey, UK), a 5 wt% Nafion ionomer solution (density, 0.874 g mL^{-1}; Sigma Aldrich, USA), deionized water, and isopropyl alcohol. To construct the anode, IrO_2 (Premion®, 99.99% metal basis, Ir 84.5% min; Alfa Aesar, USA) was used, and the catalyst ink was prepared by a homogeneous mixture of IrO_2 powder, a 5 wt% Nafion ionomer solution, deionized water, and isopropyl alcohol. During the preparation, the weight ratio of Nafion ionomer to dry mixture (solidified Nafion ionomer + IrO_2) was carefully controlled, and four types of IrO_2 catalyst inks with 5, 10, 25, and 40 wt% C_{iono} were prepared. All catalyst inks were uniformly dispersed by an ultra-sonicator and directly sprayed onto the surface of the Nafion membrane (NR212; Dupont, USA). The Pt-loading of the cathode for all samples was fixed to 0.2 mg cm^{-2} with a C_{iono} of 28 wt%. In the case of the anode, the amount of loaded IrO_2 was controlled to be 0.2, 0.5, 1.0, and 1.5 mg cm^{-2} with different C_{iono} of 5, 10, 25, and 40 wt%, respectively. To quantify the L_c, the weight difference before and after spraying the catalyst solution onto the PET film was measured ($W_{catalyst} = W_{catalyst+PET} - W_{PET}$). Finally, the prepared MEAs were dried at ambient temperature for more than 12 h.

Pretreatment of the titanium felt and titanium bipolar plate

To reduce the interfacial resistance from the partially oxidized surface of the platinized Ti felt (purchased from Bekaert Toko Metal Fiber Co.) and Ti bipolar plates, an acid pretreatment was carried out at 60 °C and 80 °C, respectively, using a 5 wt% oxalic acid solution. After treatment for 1 h, the Ti felt and Ti bipolar plates were taken out from the solution and washed with deionized water to remove the residual oxalic acid. An SEM image of the Ti felt and a digital camera image of the Ti bipolar plate are shown in Fig. S1.

Electrochemical measurements

All of the components of a single cell comprising the two different bipolar plates made of Ti and graphite, Teflon gaskets, Ti felt, a gas diffusion layer (GDL; 39BC, SGL, Germany), and the prepared MEA were tightly assembled by applying a torque of 80 ft lbs. The bipolar plates on both sides had a serpentine-type flow path with a 1 mm width and height. In the single-cell assembly, the Ti bipolar plate and Ti felt were implemented at the anode side, and the graphite bipolar plate and GDL were used at the cathode side. The assembled single cell was connected with the PEMWE test station (CNL, Korea) and a potentiostat (HCP-803; BioLogic, France). To fully hydrate the MEA and stabilize the operating conditions at 80 °C, 20 mL of deionized water and 300 sccm of nitrogen (N_2) gas were supplied to the anode and cathode, respectively, while the operating temperature was raised to 80 °C. When the temperature was sufficiently stabilized, the N_2 supply was stopped, and the flow rate of the deionized water was maintained at 20 mL during the electrochemical measurements. Then, the I–V polarization curve was recorded at an interval of 1 s via voltage scanning from 1.35 to 2.1 V at a rate of 2 mV s^{-1}. The HFR was measured at a fixed frequency of 2.5 kHz, and the EIS response was obtained at 1.6 and 1.9 V with an amplitude of 50 mV within a frequency range of 0.1–15 kHz under the same operating conditions. Cyclic voltammograms were measured between 0.05 and 1.40 V at a scan rate of 50 mV s^{-1} to calculate the electrochemical surface area (ECSA) of the anode (i.e., the IrO_2 electrode) at room temperature. During the CV measurements, 50 sccm of H_2 and N_2 was supplied into the cathode (the reference and counter electrode) and the anode (the working electrode), respectively.

Characterization. The structural characteristics of the Ti felt and the MEAs with different L_c and C_{iono} were investigated using field-emission SEM (FE-SEM; HITACHI, SU-5000).

Results and discussion

The polymer electrode membrane water electrolysis performance of the 16 prepared membrane electrode assemblies

Fig. 1 shows a schematic of the single PEMWE cell, as well as the electrode configuration comprising an IrO_2 catalyst and Nafion ionomer on the anode. As shown in Fig. 1a, in a PEMWE system, water molecules are supplied as a reactant to the anode, and a voltage is applied to produce O_2 at the anode side through the OER. The protons generated by the OER then migrate to the cathode and pass through the membrane while electrons are supplied to the cathode through an external wire, leading to the production of H_2 gas at the cathode side by the HER. Compared with the rapid kinetics of the HER at the cathode, the much slower kinetics of the OER take up a substantial portion of the overall voltage losses of the PEMWE. Therefore, optimizing the anode CL structure, comprising the IrO_2 catalyst, Nafion ionomer, and pores, is necessary (Fig. 1b).

Since the L_c and C_{iono} in the anode electrode are the critical factors determining the overall MEA performance of the PEMWE, a comprehensive study was conducted herein to determine the optimal conditions for acquiring superior performance by considering the interdependence between the two factors. To achieve this, 16 experimental sets were prepared through a cross combination of Nafion C_{iono} (5, 10, 25, and 40 wt%) and IrO_2 anode L_c (0.2, 0.5, 1.0, and 1.5 mg cm^{-2}). The Nafion C_{iono} of the cathode CLs was fixed to 28 wt% for all the experimental sets. Experimental details regarding the preparation and fabrication for each case are provided in the experimental section. Fig. 2a and b shows the three-dimensional plots used to compare the performance of each of the 16 prepared MEAs with variations in L_c and C_{iono} at a low voltage of 1.45 V (Fig. 2a) and a high voltage of 1.9 V (Fig. 2b).

Interestingly, the MEAs that exhibited the best performance were different at each working voltage. At a low working voltage of 1.45 V, the current density (proportional to the production rate of O_2 and H_2 gases) tended to increase as the L_c increased given the same C_{iono}, exhibiting the highest performance of 0.128 A cm^{-2} at a C_{iono} of 10 wt% and an L_c of 1.5 mg cm^{-2}. However, at a high working voltage of 1.9 V, the current density did not increase linearly with the L_c, as was observed at a low working voltage. The highest performance of 4.834 A cm^{-2} was exhibited at a C_{iono} of 10 wt% and an L_c of 0.5 mg cm^{-2}, which was one-third of the L_c at a low working voltage. In addition, the optimal L_c was different for each C_{iono} of 5, 10, 25, and 40 wt%, indicating that the two experimental

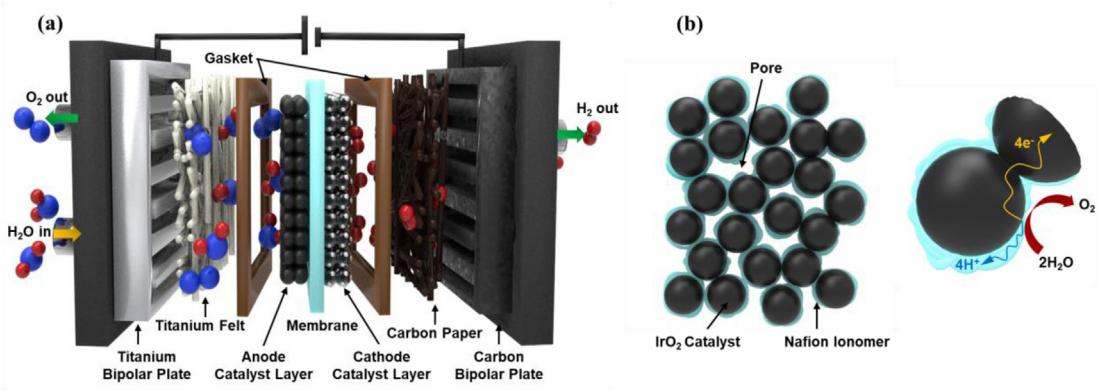

Fig. 1 – (a) A schematic of the PEMWE single cell and (b) the electrode configurations on the anode.

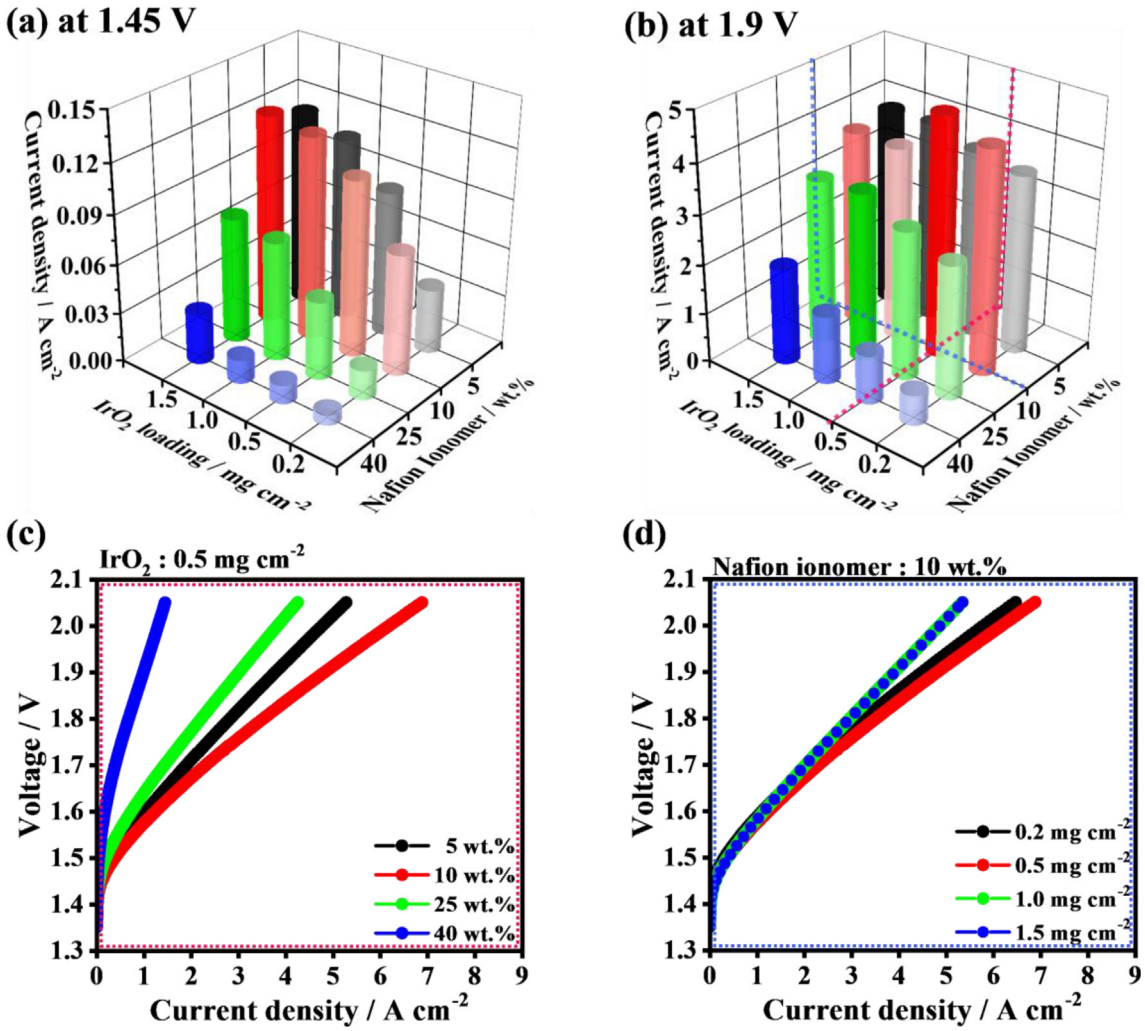

Fig. 2 – (a–b) Three-dimensional plots for the PEMWE performance with variations in L_c and Nafion C_{iono} at (a) 1.45 V and (b) 1.9 V. (c–d) The polarization curves of (c) the MEAs with variations in C_{iono} and a fixed L_c of 0.5 mg cm^{-2}; (d) the MEAs with variations in L_c and a fixed C_{iono} of 10 wt%.

factors were inter-dependent and highlighting the need for considering the two factors simultaneously according to the working environment of the PEMWE. The I–V performances at 1.45 and 1.9 V with varied C_{iono} and L_c are summarized in Table 1. To examine the I–V response for all the working voltage regions, we selected a fixed condition including an L_c of 0.5 mg cm^{-2} (Fig. 2c) and a C_{iono} of 10 wt% (Fig. 2d), respectively, referring to the results for the best PEMWE performance.

Table 1 – A summary of the I–V performance at 1.45 and 1.9 V with variable C_{iono} and L_c values.

Current density [A cm^{-2}]	IrO_2	Ionomer			
		5 wt%	10 wt%	25 wt%	40 wt%
1.45 V	0.2 mg cm^{-2}	0.0396	0.0741	0.0180	0.0063
	0.5 mg cm^{-2}	0.0893	0.1080	0.0479	0.0114
	1.0 mg cm^{-2}	0.1116	0.1241	0.0729	0.0145
	1.5 mg cm^{-2}	**0.1190**	**0.1277**	**0.0770**	**0.0309**
1.9 V	0.2 mg cm^{-2}	3.6349	4.5140	2.7000	0.6101
	0.5 mg cm^{-2}	3.7888	**4.8344**	3.0040	0.9835
	1.0 mg cm^{-2}	**4.0428**	3.9121	**3.4058**	1.3807
	1.5 mg cm^{-2}	4.0252	3.9219	3.3292	**1.9618**

Based on the I–V plots, the maximum current density of the MEA was found to be 6.882 A cm^{-2} at 2.05 V, which was a very high performance in comparison with previously reported PEMWE performances (Table S1). Based on these results from our 16 experimental sets, we confirmed that the C_{iono} significantly affected the PEMWE performance over the entire working voltage region, while it is a limit regarding an increasing L_c in the high-working-voltage region, where severe mass transport resistance occurred.

Overpotentials of polymer electrode membrane water electrolysis

Because the performance of PEMWE was determined by three main overpotentials, we analyzed the governing equation for the operating cell voltage of the PEMWE system to investigate the effects of C_{iono} and L_c on the overall performance. The governing equation for the operating cell voltage can be expressed as follows [19,20]:

$$E_{cell} = E_{rev} + \eta_{kinetic} + \eta_{ohmic} + \eta_{mass} \quad (1)$$

where E_{cell} is the operating cell voltage, E_{rev} is the reversible cell voltage, $\eta_{kinetic}$ is the kinetic overpotential, η_{ohmic} is the ohmic overpotential, and η_{mass} is the mass transport overpotential. Regarding $\eta_{kinetic}$, this can be written as a function of L_c [12,21]:

$$\eta_{kinetic} = \left(\frac{RT}{\alpha nF}\right)\ln\frac{j}{j_0} = \left(\frac{RT}{\alpha nF}\right)\ln\frac{j}{L_C j_0} \quad (2)$$

where L_C is the effective L_c per unit area [g/cm^2], j_0 is the exchange current density [A/cm^2], and j_0 is the catalyst-specific exchange current density [A/g]. In this equation, it should be noted that $\eta_{kinetic}$ is inversely proportional to L_C. Next, η_{ohmic} comprises the proton transport-related resistance on the membrane, the H^+ ion transport on the ionomer chains of the CL, and the overall electrical resistance of the system. Thus, the proton transport through the CL can be represented as a function of the thickness and C_{iono} of the CL [18] as follows:

$$\eta_{ohmic} = jR_{ohmic} = j(R_{mem} + R_{H^+,\,CL} + R_{elec}) \quad (3-1)$$

$$R_{H^+,\,CL} = \frac{t_{CL}}{\sigma\, V_{ion}/\tau} \quad (3-2)$$

where t_{CL} is the thickness of the CL, V_{ion} is the ionomer volume fraction in the CL, and τ is the apparent tortuosity of the ionomer phase in the CL. The final contributing factor of the E_{cell}, i.e., η_{mass}, is expressed as a combination of the O_2 concentration difference related to the diffusion term in the low-current-density region, and the flow restriction term for the blockage of the water pathway to the active sites is represented by the growing O_2 gas bubbles in the high-current-density region as follows [20]:

$$\eta_{mass} = \frac{RT}{nF}\ln\left[\left(\frac{C_{O_2}}{C^{\circ}_{O_2}}\right) + \left(\frac{\dot{V}_r}{\dot{V}_c}\right)^2\right] \quad (4-1)$$

$$\frac{C_{O_2}}{C^{\circ}_{O_2}} \propto \frac{t_{CL}}{D^{eff}_{O_2}}\left(D^{eff}_{O_2} = \varepsilon^k D_{O_2},\ k: constant\right),$$

$$\dot{V}_r = \frac{\dot{V}_{O_2,\,prod}}{\dot{V}_{H_2O,\,sup}},\ \dot{V}_c = \frac{d_p^2}{d_p^2 - (d_p - \delta_c)^2} \quad (4-2)$$

In the above equations, C_{O_2} is the local concentration of O_2 gas at the CL, $C^{\circ}_{O_2}$ is the reference concentration of O_2 gas 298.15 K and 1 atm, which is standard temperature and pressure condition (STP), $\dot{V}_r$ is the ratio of the produced O_2 and the supplied water flow rate, and $\dot{V}_c$ is a ratio that expresses the pore diameter required for a pore to maintain a liquid pathway along its wall. Furthermore, ε is the porosity of CL, D_{O_2} is the nominal diffusivity of the O_2, D^{eff} is the effective diffusivity of the product, d_p is the given pore diameter, and δ_c is the critical water film thickness necessary for the reaction. Since the electrode comprises the identical catalyst (no difference in size and shape) and ionomer using the same fabrication method, d_p is directly affected by the change in ε due to the difference in pore filling, and they are proportional [22,23]. Therefore, it can be assumed that η_{mtx} is proportional to t_{CL} and inversely proportional to the ε of the CL.

Analysis of the catalyst layer structure and active sites related to Nafion ionomer content and catalyst loading

To determine the relationship between L_C and C_{iono} and the PEMWE voltage losses ($\eta_{kinetic}$, η_{ohmic}, and η_{mass}), as well as their contributing factors, such as L_C, V_{ion}, t_{CL}, and ε, SEM observations of a cross-section of each MEA were completed. Fig. 3a and b shows the cross-sectional SEM images of the MEAs with variations in L_C for a fixed C_{iono} of 10 wt% and the MEAs with a variation of C_{iono} given a fixed L_C of 0.5 mg cm^{-2}, respectively. Based on Fig. 3a, when the L_C increased (0.2, 0.5, 1.0, and 1.5 mg cm^{-2}), the average t_{CL} increased and reached values of approximately 2.6, 4.3, 6.8, and 8.4 μm, respectively, as was anticipated. However, the relationship between these two factors was not perfectly linear. Interestingly, when introducing the thickness per unit mass of the electrode ($t_{CL/unit\ mass}$) as an indicator for a comparison of ε, the $t_{CL/unit\ mass}$ decreased (i.e., ε was reduced) as the L_C increased as shown in Fig. 3c. This phenomenon can be viewed as a compression effect resulting from the successive impaction of the traveling particles during the spray-based electrode fabrication process and a decrease in pore volume due to the gradual filling of the pores of follow-up particles [4,24,25].

Next, when examining the geometrical features of the CL given variations in C_{iono} (5, 10, 25, and 40 wt%) and a fixed L_C at 0.5 mg cm^{-2}, the average t_{CL} of the samples was observed to be

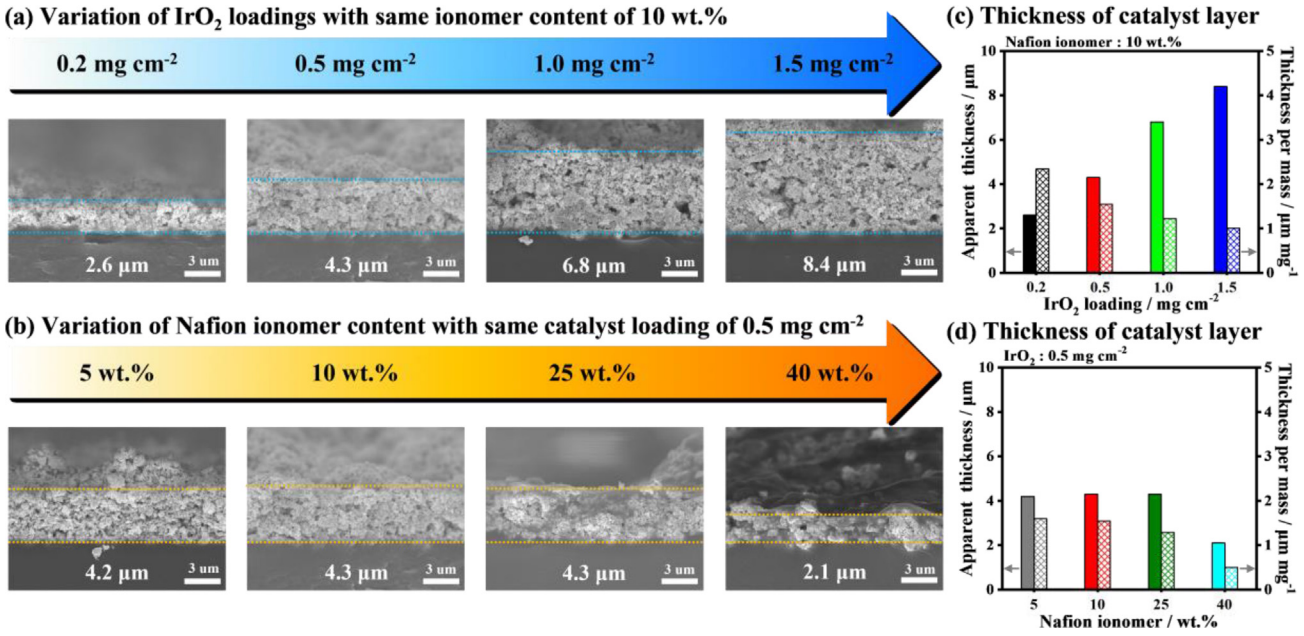

Fig. 3 – (a–b) The SEM images of the L_C with variations in (a) L_C and (b) C_{iono}. (c–d) The apparent thickness and the thickness of the CL per unit mass as a function of (c) L_C and (d) C_{iono}.

approximately 4.3 μm, as shown in Fig. 3b. The exception in this regard was for the 40 wt% C_{iono} case, which had a significantly reduced thickness of 2.1 μm. This was attributed to the fact that the excessive C_{iono} filled up the macro-pores in the CL, binding each catalyst particle together and, in turn, giving rise to a densified electrode structure [18,23]. When comparing the $t_{CL/unit\ mass}$ values (Fig. 3d), the C_{iono} values of 5, 10, 25, and 40 wt % led to values of 1.59, 1.55, 1.29, and 0.50 μm, respectively, indicating that the use of a large C_{iono} (≥ 25 wt%) resulted in a reduction of ε. Based on these results, it was concluded that the ε of the CL decreased as L_C and the C_{iono} increased, and the t_{CL} increased with an increment in the L_C.

Considering that the L_c and C_{iono} of the anodic electrode could influence the morphological properties (e.g., thickness and porosity) of the MEA as shown in Fig. 3, the contributing factors of L_c and C_{iono} influenced the ECSA of the MEAs, which would determine the $\eta_{kinetic}$. To compare the ECSA of each MEA, which directly affected the $\eta_{kinetic}$, CV measurements were carried out. The number of electrochemically active sites available for the OER could be determined by CV charge in total q, which was obtained from the integration of the CV curve between 0.05 and 1.40 V [12,18]. Fig. 4a and b shows the CV curves for the anode side of the prepared MEAs achieved by varying the L_C with a fixed C_{iono} of 10 wt% (Fig. 4a) and by varying the C_{iono} with a fixed L_C of 0.5 mg cm^{-2} (Fig. 4b). For the effect of the L_C with a fixed C_{iono}, total voltammetric charge, q, exhibited a proportional relation with the L_C due to an increase in the number of active sites per unit area, and the calculated values were 2.7243C (0.2 mg cm^{-2}), 4.2294C (0.5 mg cm^{-2}), 6.8417C (1.0 mg cm^{-2}), and 8.5452C (1.5 mg cm^{-2}) as summarized in Table 2.

For varying C_{iono} with a fixed L_C, the sample with a 10 wt% exhibited the highest total voltammetric charge among the MEAs, i.e., 4.2294C; this value was even larger than the MEA with a C_{iono} of 5 wt% due to the formation of a better proton-conducting network in the CL. However, the high C_{iono} values of 25 and 40 wt% led to much lower total voltammetric charges of 2.5337 and 0.2738C, respectively, indicating that the ECSA was being reduced, assuming that the number of active sites for the OER was proportional to the total voltammetric charge [18]. The total voltammetric charge of the sample with a C_{iono} of 40 wt% was particularly low compared with the others because the surface of the catalyst was severely blocked by the excessive C_{iono}, as is shown in the cross-sectional SEM image in Fig. 3b. To find out the impact of C_{iono} in the electrode on the $\eta_{kinetic}$, EIS analysis of the MEAs with C_{iono} of 5, 10, 25, and 40 wt% with fixed IrO_2 loading of 0.5 mg cm^{-2} were performed under a low working voltage region of 1.6 V (Fig. S2). At low working voltage, charge transfer resistance is dominant compared to mass transport resistance, therefore, the diameter of the semi-circle can be considered as $\eta_{kinetic}$ related to charge transfer resistance [26]. As shown in Fig. S2, the diameter of the semi-circle was the smallest for the MEA with C_{iono} of 10 wt% and calculated charge transfer resistances are 0.0495, 0.0531, 0.0725, and 0.6502 Ω cm^2 for C_{iono} of 10, 5, 25, and 40 wt%, respectively (Table S2). This result is consistent with the trend of difference in the relative ECSA values. Notably, in the case of the MEA with C_{iono} of 40 wt%, it can be seen that the charge transfer is severely inhibited due to excessive ionomer content, which can cause additional significant mass transport resistance at a high working voltage [27,28], and it will be described in Section Electrical and gas percolation depending on Nafion ionomer content and catalyst loading. The effect of the measured total voltammetric charge on the performance was also confirmed by Tafel slopes in the polarization curve in the low-current-density region. The Tafel slopes for each MEA were extracted from the IR-corrected I–V curves as shown in Fig. 5a and b. The Tafel slope decreased with an increasing L_C under a fixed C_{iono}, and when the L_C was fixed, a

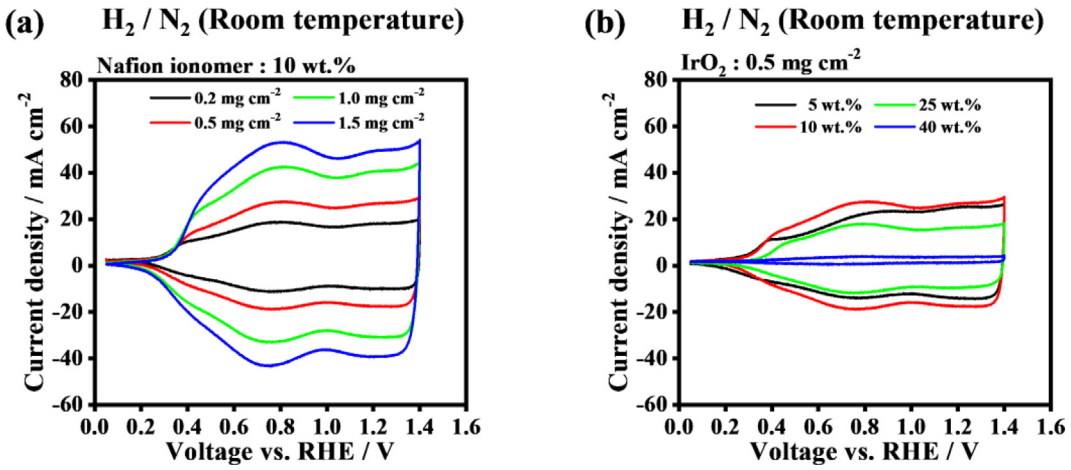

Fig. 4 – Cyclic voltammograms of IrO_2-based anodes with (a) different L_C values and (b) Nafion C_{iono}.

Table 2 – The voltammetric charge in total calculated from CVs with variations in L_C.

IrO_2 [mg_{Ir} cm^{-2}] with ionomer content of 10 wt%	0.2	0.5	1.0	1.5
Voltammetric charge in total [C]	2.7243	4.2294	6.8417	8.5452
Ionomer content [wt.%] with IrO_2 loading of 0.5 mg cm^{-2}	5	10	25	40
Voltammetric charge in total [C]	3.5581	4.2294	2.5337	0.2738

C_{iono} of 10 wt% led to the smallest value of 47.0 mV dec^{-1}. These results corresponded well with the measured voltammetric charge trends derived from the CV spectra and indicated that the appropriate C_{iono} and L_C should be simultaneously considered to obtain a high-performance and a well-constructed CL with a suitable ε and ECSA.

Electrical and gas percolation depending on Nafion ionomer content and catalyst loading

Nafion ionomer acts as a proton-conducting material, but it can also serve as an insulating binder in the CL. In Fig. 3b, it is clearly shown that the Nafion ionomers in the catalyst layers with C_{iono} of 10 wt% or less were uniformly coated on the surface of the IrO_2 particles without severe agglomeration, however, in the catalyst layers with C_{iono} above 25 wt%, agglomerated ionomers and even thin-ionomer layer on the electrode surface were observed. Consequently, high ionomer contents over 25 wt% can block the electron transfer pathway in the CL as well as the interface between the CL and the porous transport layer (PTL), in turn, it results in the increase of $\eta_{ohmic.}$. Next, to determine the effect of the ε of the CL on η_{mass}, the capillary effect of the small pores was considered. The generated O_2 gas initially became stuck to the CL. Oxygen gas cannot escape the pores when its pressure is lower than the capillary pressure (P_c), which is defined as follows [29].

$$P_c = \frac{2\gamma \cos\theta}{r_c} \quad (5)$$

where θ is the contact angle, γ is the surface tension, and r_c is the pore radius. This equation indicates that the required gas pressure for invading neighboring pores (i.e., $P \geq P_c$) increased as the pore (or throat) size decreased. The number of dead pores due to gas bubbles stuck in the CL was also much greater in the case of a reduced ε in the same pressure conditions.

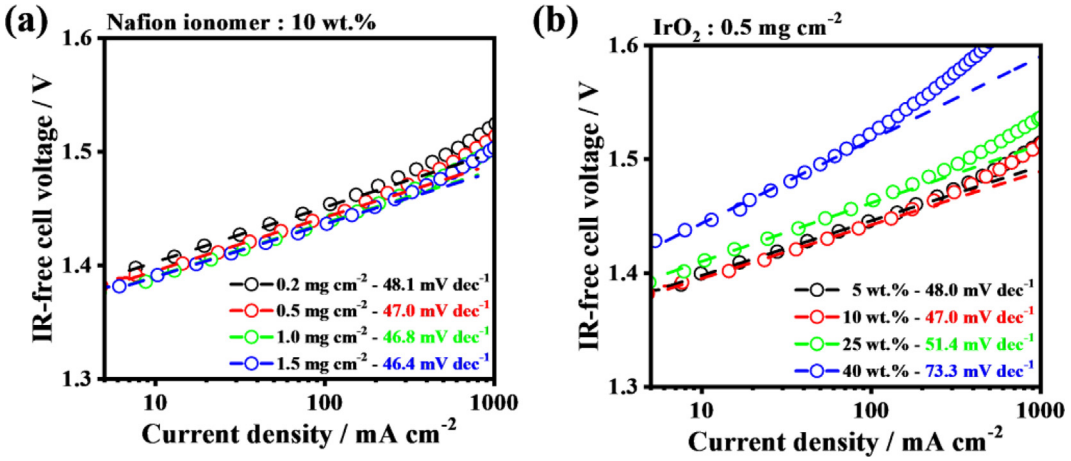

Fig. 5 – Tafel plots of the MEAs with variations in (a) Nafion C_{iono} and (b) L_c values.

Therefore, it is critical to guarantee an acceptable value of ε in the CL, which is affected by C_{iono} and the L_c, while simultaneously securing high electrical conduction, ionic transport, and ECSA.

To electrochemically verify the effects of inhibited electron transfer and gas percolation on the η_{ohmic} and η_{mass}, HFR measurements for the overall-current-density region and EIS spectra at 1.9 V were conducted for MEAs with varying C_{iono} and a fixed L_c of 0.5 mg cm^{-2} (see Fig. 6a and b) and with varying L_c and a fixed C_{iono} of 10 wt% (Fig. 6c and d). As shown in Fig. 6a, the MEA with a C_{iono} of 10 wt% exhibited the lowest HFR of approximately 65.4 mΩ cm^2 over the measured current density range. For the MEA with a C_{iono} of 5 wt%, an ~31.2% higher HFR value (~85.8 mΩ cm^2) was shown compared with a C_{iono} of 10 wt%, which indicated that a C_{iono} of 5 wt% was not sufficient for forming a proton-conducting network in the CL (due to a decreased V_{ion}). Concurrently, the HFR value of the MEA with a C_{iono} of 40 wt% was much higher (hundreds of mΩ cm^2), and that of the MEA with a C_{iono} of 25 wt% was nearly twice that of the MEA with a C_{iono} of 10 wt%, which was attributed to the inhibited electron transfer effect as noted above. This result was confirmed by the EIS spectra measured at 1.9 V as shown in Fig. 6b. The intercept with the real axis represents the ohmic resistance in the PEMWE. The results indicate that an excessive C_{iono} significantly increase η_{ohmic} due to inhibited electron transfer in the CL and the CL|PTL interface. Therefore, it is important to lower the ohmic resistance while securing proper ionic and electronic conductivity through optimization of the ionomer content in the electrode. Also, it is worthwhile to mention that, the MEA with a C_{iono} of 40 wt%, showed a much larger diameter of the semi-circle in the EIS spectra compared to other MEAs under high working voltage of 1.9 V where the mass transport is severely restricted. It is attributed to that excessive C_{iono} would induce severe void volume reduction (low ε) in the CL, and thus, result in the formation of trapped oxygen bubbles in the CL and it blocks the reactant supply.

For the effect of L_c with a fixed C_{iono} of 10 wt% (see Fig. 6c and d), the MEA with an L_c of 0.5 mg cm^{-2} exhibited the lowest HFR of ~65.4 mΩ cm^2 among those in the experimental set. The MEAs with high L_c values of 1.0 and 1.5 mg cm^{-2} exhibited ~25.1% and ~24.3% higher HFR values, respectively, than the MEAs with a 0.5 mg cm^{-2} value, which was attributed to the increased η_{ohmic} for proton transport through the CL caused by the increased t_{CL}. It is worth noting that the HFR values of the MEAs with relatively high L_c values (1.0 and 1.5 mg cm^{-2}) increased as the current density increased, whereas the MEAs with relatively low L_c groups (0.2 and 0.5 mg cm^{-2}) maintained

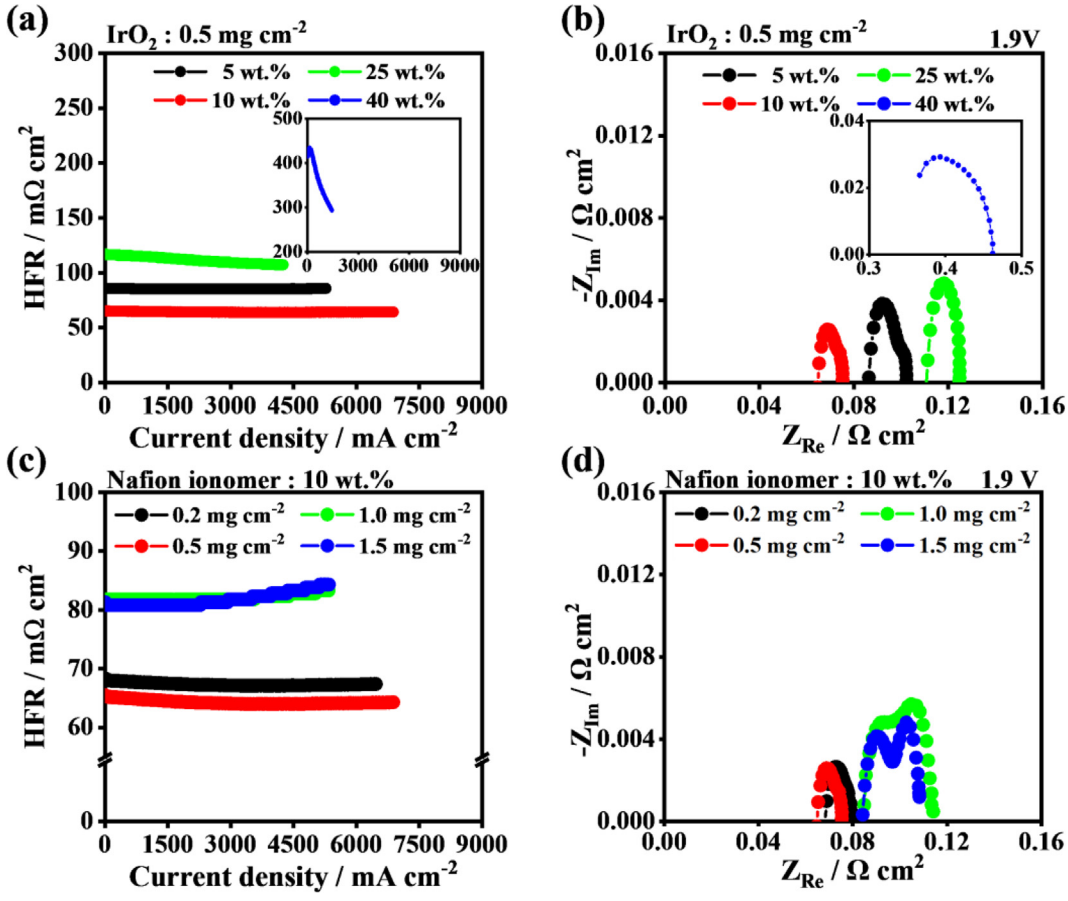

Fig. 6 – (a, c) The HFR spectra and (b, d) EIS spectra for (a, b) MEAs with variable C_{iono} given a fixed L_c of 0.5 mg cm^{-2}, and (c, d) the MEAs with variable L_c given a fixed C_{iono} of 10 wt%.

Table 3 – A summary of the effect of the different C_{iono} and L_c on each overpotential factor.

Representative overpotentials	$\eta_{kinetic}$	η_{ohmic}			η_{mtx}	
		$R_{H+,\,CL}$		R_{elec}		
Contributing factors	Electrochemical surface area	Electrode thickness	Ionomer Volume	Electron transfer	Electrode thickness	Porosity
C_{iono} ↑ (ionomer content)	↓ (≤ 10 wt%) ↑ (≥ 10 wt%)	– (except for 40 wt%)	↓	↑	– (except for 40 wt%)	↑
L_c ↑ (catalyst loading)	↓	↑	–	–	↑	↑
Correlation effect	↓ (≤ 10 wt% C_{iono}) ↑ (≥ 10 wt% C_{iono})	↓ or ↑			↑	

their initial HFR. This result infers that the η_{mass} was significantly involved in the MEA with a high L_c due to the increased t_{CL} and the reduced ε of the densified CL. This hampered the ionic transport and reactant supply, resulting in an increased HFR in the high-current-density region (i.e., a large amount of trapped O_2 gas in the pores). This was further confirmed by the EIS spectra at 1.9 V shown in Fig. 6d, where the MEAs in the high-L_c group have a much larger diameter than those in the low-L_c group.

Correlation effects between catalyst loading and ionomer content on polymer electrode membrane water electrolysis performance

Based on these observations, the effects of the L_c and C_{iono} on the representative PEMWE voltage losses ($\eta_{kinetic}$, η_{ohmic}, and η_{mass}) were summarized considering their contributing factors including the L_C and ECSA for $\eta_{kinetic}$, the t_{CL} and V_{ion} for η_{ohmic}, and the t_{CL} and ε for η_{mass} as shown in Table 3. The positive and negative effects on the performance are highlighted in red and blue, respectively, and with downward and upward arrows, respectively. First, as the major contributing factor to $\eta_{kinetic}$, the ECSA increased as the C_{iono} increased until reaching 10 wt % and decreased as the C_{iono} increased above 10 wt%. The ECSA was also proportional to the degree of L_C. Regarding η_{ohmic}, which comprised $R_{H^+,\,CL}$ and R_{elec}, an increase in C_{iono} had a positive effect on the decrease of $R_{H^+,\,CL}$, which was achieved by an increase in V_{ion} due to the securing of additional proton conduction pathways. However, if an excessive C_{iono} was incorporated into the CL, it adversely affected the increase of R_{elec} due to the inhibited electron transfer effect. In addition, the increased L_c resulted due to an increment in t_{CL}, which induced an increment in $R_{H^+,\,CL}$. For the η_{mass}, a high C_{iono} could significantly reduce the ε by blocking the pores in the CL. The thickening and densification of the electrode due to the increased L_c also reduced the ε and increased the length of the pathway for the reactant and the product. Because the C_{iono} and L_c simultaneously induced an increased mass transport loss through the reduced ε of the CL, it was inferred that there would be a limit in the increases possible for each of the two factors.

Finally, to verify the correlation effects of C_{iono} and L_c on the PEMWE performance, the current density of each MEA was represented at a low (1.45 V) and high voltage (1.9 V), respectively. This was based on the $\eta_{kinetic}$ being more dominant than the η_{ohmic} and η_{mass} in the low-working-voltage region, whereas the η_{mass} and η_{ohmic} were dominant in the high-working-voltage region. Fig. 7a–h shows the plots for the current densities at specific voltages of 1.45 and 1.9 V for the MEAs with varying C_{iono} and a fixed L_c value (Fig. 7a–d) and with a varying L_c value and a fixed C_{iono} (Fig. 7e–h). Regarding the C_{iono} at a low working voltage of 1.45 V (Fig. 7a–d), the MEAs with a C_{iono} of 10 wt% showed the highest performance regardless of the L_c value. The performance then decreased sharply, beginning with the MEA with a C_{iono} of 25 wt%, compared with those with a C_{iono} of 5 or 10 wt%. The higher performance of the MEA with a C_{iono} of 10 wt% under a low working voltage of 1.45 V was attributed to the decreased $\eta_{kinetic}$ caused by the increased ECSA; this indicated that a 10 wt% C_{iono} was beneficial for the formation of an appropriate tri-phase (proton, electron, and water) interface in the CL. Furthermore, regarding the L_c (Fig. 7e–h), the performances of all the MEAs were proportional to the L_c regardless of C_{iono} due to the decreased $\eta_{kinetic}$ caused by the increased number of volumetric active sites (i.e., increased ECSA).

In the high-working-voltage region, where η_{mass} and η_{ohmic} dominantly affected the PEMWE performance, a different performance trend was observed compared with the low-working-voltage region. For C_{iono} (Fig. 7a–d), the MEAs were classified into two groups, i.e., one with a relatively low L_c (0.2 and 0.5 mg cm^{-2}) and one with a relatively high L_c (1.0 and 1.5 mg cm^{-2}). The low-L_c group still exhibited the highest performance with a C_{iono} of 10 wt%. Concurrently, the high-L_c group exhibited the highest performance with a C_{iono} of 5 wt%. This trend was ascribed to the correlation effect of the C_{iono} and L_c for η_{mass}, which was inversely proportional to the ε of the CL. Since increasing the C_{iono} and L_c superpositionally induced the reduction of ε, the peak performance shifted to a lower value of C_{iono} as L_c increased; this highlighted the existence of a lower limit for ε, particularly at high working voltages. In addition, a rapid performance drop in the MEAs with a C_{iono} of 25 and 40 wt% was observed due to inhibited electron transfer effect. This means that non only $R_{H^+,\,CL}$ but also R_{elec} should be simultaneously considered for reducing overall η_{ohmic}. For the effect of L_c at a high working voltage (Fig. 7e–h), the peak performances of the MEAs with C_{iono} values of 5 and 10 wt% and an optimum L_c were reversed from 1.0 to 0.5 mg cm^{-2}. This further confirmed the importance of the correlation effect of C_{iono} and L_c on η_{mass} , based on a simultaneous change in the ε of the CL.

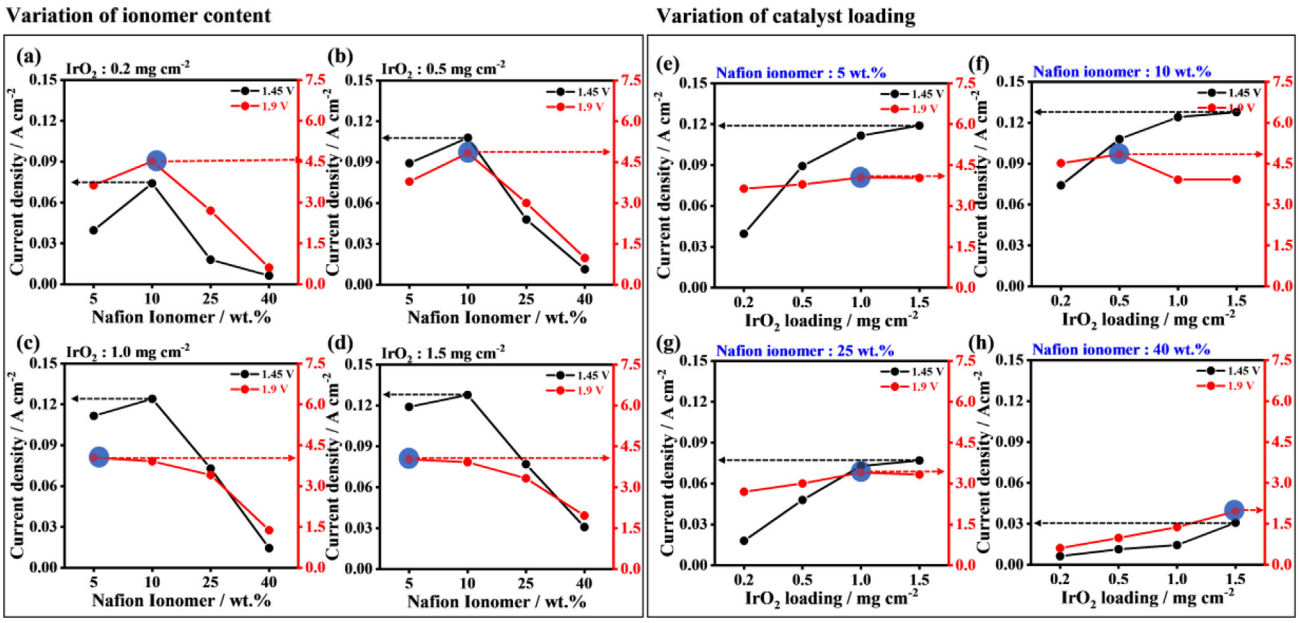

Fig. 7 – (a–h) The current density at 1.45 and 1.9 V for fixed L_c amounts of (a) 0.2, (b) 0.5, (c) 1.0, and (d) 1.5 mg cm^{-2} with varying Nafion C_{iono} and for fixed C_{iono} of (e) 5 wt%, (f) 10 wt%, (g) 25 wt%, and (h) 40 wt% with varying L_c amounts.

Conclusion

In this study, a comprehensive investigation of the effects of L_c and C_{iono} was conducted using 16 MEAs comprising a cross-combination of two experimental factors. To analyze the PEMWE performance with respect to the kinetic, ohmic, and mass transfer overpotentials, we considered the ECSA, ionomer volume fraction, thickness, and porosity of the electrode as contributing factors, which were dependent on the L_c and C_{iono}. At a low working voltage of 1.45 V, where the kinetic loss was dominant, the PEMWE performance depended on the ECSA. Accordingly, it exhibited a proportional relationship with the L_c amount, and the optimal C_{iono} was 10 wt%, regardless of the L_c. This indicated that the correlation effects between L_c and C_{iono} were not dominant in the low overpotential region. However, at a high working voltage of 1.9 V, where the mass transfer and ohmic losses were dominant, correlation effects between the L_c and C_{iono} on the PEMWE performance were observed. This was attributed to the C_{iono} and L_c being able to superpositionally affect porosity changes in the electrode, which was significantly linked to the mass transfer of the system. In addition, the optimal C_{iono} was changed to achieve the best performance, based on the L_c and vice versa. These results highlighted the existence of a lower limit for the porosity with which to obtain the best possible performance in the high-working-voltage region. Furthermore, a rapid drop in performance was observed when the C_{iono} exceeded 25 wt%, at which point the inhibited electron transfer caused the severe ohmic loss. Finally, a high-performance PEMWE (6.882 A cm^{-2} at 2.05 V) was achieved with an optimized CL structure including a low L_c of 0.5 mg cm^{-2} and a C_{iono} of 10 wt%.

Declaration of competing interest

The authors declare that they have no known competing financial interests or personal relationships that could have appeared to influence the work reported in this paper.

Acknowledgments

This work was funded by the Korea Electric Power Corporation (grant number: R21XO01-2) and the National Research Foundation (NRF) of Korea (2021M3H4A1A02042957).

Appendix A. Supplementary data

Supplementary data to this article can be found online at https://doi.org/10.1016/j.ijhydene.2022.04.019.

REFERENCES

[1] Niether C, Faure S, Bordet A, Deseure J, Chatenet M, Carrey J, et al. Improved water electrolysis using magnetic heating of FeC-Ni core-shell nanoparticles. Nat Energy 2018;3:476–83. https://doi.org/10.1038/s41560-018-0132-1.

[2] Staffell I, Scamman D, Velazquez Abad A, Balcombe P, Dodds PE, Ekins P, et al. The role of hydrogen and fuel cells in the global energy system. Energy Environ Sci 2019;12:463–91. https://doi.org/10.1039/c8ee01157e.

[3] Klose C, Saatkamp T, Münchinger A, Bohn L, Titvinidze G, Breitwieser M, et al. All-hydrocarbon MEA for PEM water electrolysis combining low hydrogen crossover and high

efficiency. Adv Energy Mater 2020;10. https://doi.org/10.1002/aenm.201903995.
[4] Babic U, Nilsson E, Pătru A, Schmidt TJ, Gubler L. Proton transport in catalyst layers of a polymer electrolyte water electrolyzer: effect of the anode catalyst loading. J Electrochem Soc 2019;166:F214–20. https://doi.org/10.1149/2.0341904jes.
[5] Cao L, Yu IKM, Xiong X, Tsang DCW, Zhang S, Clark JH, et al. Biorenewable hydrogen production through biomass gasification: a review and future prospects. Environ Res 2020;186. https://doi.org/10.1016/j.envres.2020.109547.
[6] Li J, Cheng W. Comparative life cycle energy consumption, carbon emissions and economic costs of hydrogen production from coke oven gas and coal gasification. Int J Hydrogen Energy 2020;45:27979–93. https://doi.org/10.1016/j.ijhydene.2020.07.079.
[7] Lee BS, Park HY, Choi I, Cho MK, Kim HJ, Yoo SJ, et al. Polarization characteristics of a low catalyst loading PEM water electrolyzer operating at elevated temperature. J Power Sources 2016;309:127–34. https://doi.org/10.1016/j.jpowsour.2015.12.139.
[8] Stiber S, Balzer H, Wierhake A, Wirkert FJ, Roth J, Rost U, et al. Porous transport layers for proton exchange membrane electrolysis under extreme conditions of current density, temperature, and pressure. Adv Energy Mater 2021;11. https://doi.org/10.1002/aenm.202100630.
[9] Dincer I, Acar C. Review and evaluation of hydrogen production methods for better sustainability. Int J Hydrogen Energy 2014;40:11094–111. https://doi.org/10.1016/j.ijhydene.2014.12.035.
[10] Bühler M, Hegge F, Holzapfel P, Bierling M, Suermann M, Vierrath S, et al. Optimization of anodic porous transport electrodes for proton exchange membrane water electrolyzers. J Mater Chem 2019;7:26984–95. https://doi.org/10.1039/c9ta08396k.
[11] Rozain C, Mayousse E, Guillet N, Millet P. Influence of iridium oxide loadings on the performance of PEM water electrolysis cells: Part II - advanced oxygen electrodes. Appl Catal B Environ 2016;182:123–31. https://doi.org/10.1016/j.apcatb.2015.09.011.
[12] Rozain C, Mayousse E, Guillet N, Millet P. Influence of iridium oxide loadings on the performance of PEM water electrolysis cells: Part I-Pure IrO2-based anodes. Appl Catal B Environ 2016;182:153–60. https://doi.org/10.1016/j.apcatb.2015.09.013.
[13] Reddi K, Elgowainy A, Rustagi N, Gupta E. Impact of hydrogen refueling configurations and market parameters on the refueling cost of hydrogen. Int J Hydrogen Energy 2017;42:21855–65. https://doi.org/10.1016/j.ijhydene.2017.05.122.
[14] Fuentes RE, Farell J, Weidner JW. Multimetallic electrocatalysts of Pt, Ru, and Ir supported on anatase and rutile TiO2 for oxygen evolution in an acid environment. Electrochem Solid State Lett 2011;14. https://doi.org/10.1149/1.3528163.
[15] Kadakia K, Datta MK, Velikokhatnyi OI, Jampani P, Park SK, Saha P, et al. Novel (Ir,Sn,Nb)O2 anode electrocatalysts with reduced noble metal content for PEM based water electrolysis. Int J Hydrogen Energy 2012;37:3001–13. https://doi.org/10.1016/j.ijhydene.2011.11.055.
[16] Marshall AT, Sunde S, Tsypkin M, Tunold R. Performance of a PEM water electrolysis cell using Irx Ruy Taz O2 electrocatalysts for the oxygen evolution electrode. Int J Hydrogen Energy 2007;32:2320–4. https://doi.org/10.1016/j.ijhydene.2007.02.013.
[17] Pham C van, Bühler M, Knöppel J, Bierling M, Seeberger D, Escalera-López D, et al. IrO2 coated TiO2 core-shell microparticles advance performance of low loading proton exchange membrane water electrolyzers. Appl Catal B Environ 2020;269. https://doi.org/10.1016/j.apcatb.2020.118762.
[18] Bernt M, Gasteiger HA. Influence of ionomer content in IrO 2/TiO 2 electrodes on PEM water electrolyzer performance. J Electrochem Soc 2016;163:F3179–89. https://doi.org/10.1149/2.0231611jes.
[19] Bazylak A, Lee JK, Lee CH, Fahy KF, Kim PJ, Krause K, et al. Accelerating bubble detachment in porous transport layers with patterned through-pores. ACS Appl Energy Mater 2020;3:9676–84. https://doi.org/10.1021/acsaem.0c01239.
[20] Fritz DL, Mergel J, Stolten D. PEM electrolysis simulation and validation. ECS Trans 2014;58:1–9. https://doi.org/10.1149/05819.0001ecst.
[21] Lee J, Seol C, Kim J, Jang S, Kim SM. Optimizing catalyst loading ratio between the anode and cathode for ultralow catalyst usage in polymer electrolyte membrane fuel cell. Energy Technol 2021;9. https://doi.org/10.1002/ente.202100113.
[22] Okumura M, Noda Z, Matsuda J, Tachikawa Y, Nishihara M, Lyth SM, et al. Correlating cathode microstructure with PEFC performance using FIB-SEM and TEM. J Electrochem Soc 2017;164:F928–34. https://doi.org/10.1149/2.0581709jes.
[23] Suzuki T, Tsushima S, Hirai S. Effects of Nafion® ionomer and carbon particles on structure formation in a proton-exchange membrane fuel cell catalyst layer fabricated by the decal-transfer method. Int J Hydrogen Energy 2011;36:12361–9. https://doi.org/10.1016/j.ijhydene.2011.06.090.
[24] Shukla S, Stanier D, Saha MS, Stumper J, Secanell M. Analysis of inkjet printed PEFC electrodes with varying platinum loading. J Electrochem Soc 2016;163:F677–87. https://doi.org/10.1149/2.1111607jes.
[25] Zhao J, Ozden A, Shahgaldi S, Alaefour IE, Li X, Hamdullahpur F. Effect of Pt loading and catalyst type on the pore structure of porous electrodes in polymer electrolyte membrane (PEM) fuel cells. Energy 2018;150:69–76. https://doi.org/10.1016/j.energy.2018.02.134.
[26] Jorge AB, Dedigama I, Miller TS, Shearing P, Brett DJL, McMillan PF. Carbon nitride materials as efficient catalyst supports for proton exchange membrane water electrolyzers. Nanomaterials 2018;8:432. https://doi.org/10.3390/nano8060432.
[27] Majasan JO, Iacoviello F, Cho JIS, Maier M, Lu X, Neville TP, et al. Correlative study of microstructure and performance for porous transport layers in polymer electrolyte membrane water electrolysers by X-ray computed tomography and electrochemical characterization. Int J Hydrogen Energy 2019;44:19519–32. https://doi.org/10.1016/j.ijhydene.2019.05.222.
[28] Schuler T, Kimura T, Schmidt TJ, Büchi FN. Towards a generic understanding of oxygen evolution reaction kinetics in polymer electrolyte water electrolysis. Energy Environ Sci 2020;13:2153–66. https://doi.org/10.1039/d0ee00673d.
[29] Schmidt G, Suermann M, Bensmann B, Hanke-Rauschenbach R, Neuweiler I. Modeling overpotentials related to mass transport through porous transport layers of PEM water electrolysis cells. J Electrochem 2020;167:114511. https://doi.org/10.1149/1945-7111/aba5d4.